Quantum manifestations of classical nonlinear resonances

Diego A. Wisniacki[1,*] and Peter Schlagheck[2]
[1]*Departamento de Física and IFIBA, FCEyN, UBA Ciudad Universitaria, Pabellón 1, Ciudad Universitaria, 1428 Buenos Aires, Argentina*
[2]*Departement de Physique, University of Liege, 4000 Liège, Belgium*
(Received 18 July 2015; published 28 December 2015)

When an integrable classical system is perturbed, nonlinear resonances are born, grow, and eventually disappear due to chaos. In this paper the quantum manifestations of such a transition are studied in the standard map. We show that nonlinear resonances act as a perturbation that break eigenphase degeneracies for unperturbed states with quantum numbers that differ in a multiple of the order of the resonance. We show that the eigenphase splittings are well described by a semiclassical expression based on an integrable approximation of the Hamiltonian in the vicinity of the resonance. The morphology in phase space of these states is also studied. We show that the nonlinear resonance imprints a systematic influence in their localization properties

DOI: 10.1103/PhysRevE.92.062923 PACS number(s): 05.45.Mt, 03.65.Sq

I. INTRODUCTION

Understanding the influence of classical structures at the quantum level is the main concern of quantum chaos [1–3]. As a mature subject, it has been the source of important results that spread in several areas of physics. For example, the universality of level fluctuations of chaotic systems conjectured in Ref. [4] and recently proved [5] has helped in understanding the level statistics of systems that range from atomic to mesoscopic size. Quantum transport is another example in which the classical integrable or chaotic behavior has a strong effect on the quantum behavior [6].

Much less studied but ubiquitous are mixed systems. The phase space of these systems is characterized by stability islands surrounded by a chaotic sea. The transition from integrable to globally chaotic behavior is convoluted due to the fact that the border of the islands is of fractal nature. The building blocks to understand such a transition are the celebrated Kolmogorov-Arnold-Moser (KAM) and Poincaré-Birkhoff (PB) theorems [7,8]. The KAM theorem states that when an integrable system is perturbed, sufficiently irrational tori survive. On the other hand, the PB theorem establishes the fate of the resonant tori, that is, tori with a rational rotational number are destroyed, resulting in the creation of an even number of unstable and stable periodic orbits. In their vicinity, chains of islands of regularity surrounded by a chaotic separatrix organized by a homoclinic tangle are formed.

The manifestation of such a transition at the quantum level is far from obvious. Classical dynamics develops increasingly complex structures due to its fractal nature; however, the absence of trajectories in the quantum realm makes an effective diffusion (of size $\hbar$ in the phase space) blur such a behavior. Understanding the traces of these opposing effects is of paramount importance to understand several phenomena. Examples of the relevance of quantal effects of this transition are the enhancement of tunneling between symmetry related tori in the nearly integrable regime [9–14] and experiments in microwave ionization of exited hydrogen atoms [15]. More recently, the transition from integrable to mixed dynamics was studied in the quantum Harper map [16,17]. Clear signatures of nonlinear r:s resonances were shown in the eigenphases and wave functions. An r:s resonance is characterized by a chain of r islands in phase space. Here s is the number of internal oscillations around the islands' center that take place within r periods of the driving. More specifically, nonlinear resonances can produce series of avoided crossings (ACs) in the eigenphase spectra for states whose quantum numbers differ by a multiple of the order of the resonance r. The minimum gaps of the ACs for states are well described using semiclassical expressions based on the theory of resonance assisted tunneling [10]. More surprisingly, the localization properties of the eigenstates at the AC are driven by the nonlinear resonance: One of the states is localized in the island chain and the other in the vicinity of the unstable periodic orbit (PO) associated with the resonance. The excitations of the localized structure are related to the number of zeros in each island or in the vicinity of the unstable PO associated with the resonance.

In this paper we go one step further and analyze in detail the quantum manifestation of the transition from integrable to mixed dynamics in one of the exemplary models of mixed dynamics, the standard map. Regarding the morphology of wave functions, we obtain the same localization properties as shown in Refs. [16,17] in the Harper map. Eigenstates that exist near a resonance in phase space and have quantum numbers that differ by a multiple of the order of the resonance ($\Delta n = rl$, with r the order of the resonance and l an integer) are organized in pairs; one of the states is localized in the island chain and the other on the corresponding unstable PO. The Husimi distribution of the state localized in the island chain has r zeros on the unstable PO and $r(l-1)$ zeros inside the islands. The other state has rl zeros in the islands (l zeros in each island of the chain). While these states are degenerate when the parameter that controls the perturbation is zero, they become energetically separate as the perturbation increases and the classical resonance occupies more and more volume in the phase space. We show that the splittings between the eigenphases of these states are very well described by a semiclassical formula that is based on the theory of resonance assisted tunneling [10–13].

The paper is organized as follows. In Sec. II we introduce the classical and quantum standard map. In Sec. III we show that due to the presence of a classical nonlinear resonance,

*wisniacki@df.uba.ar

pairs of degenerate eigenphases split as the perturbation increases. We compute the splittings between these states using a semiclassical theory. Section IV is devoted to showing the particular morphology of eigenstates that are localized in the vicinity of a nonlinear resonance. We show the systematic bias that the resonance imprints over the Husimi distribution of the eigenstates. We summarize in Sec. V.

II. STANDARD MAP

Classical and quantum maps have been very important in the development of dynamical systems. Their simple equations of motion have helped in the understanding of many important phenomena. In this regard, the standard map is a paradigmatic example that describes the generic transition from integrable to completely chaotic behavior [18]. Its universal behavior can describe interesting systems such as charged particle confinement in magnetic traps, particle dynamics in accelerators, electron magnetotransport in a resonant tunneling diode, and dynamical localization for ionization of excited hydrogen atoms in a microwave field [15,19–22].

The standard map is a two-dimensional area-preserving map that in the unit square is given by

$$\begin{aligned} p_{n+1} &= p_n + (k/2\pi)\sin(2\pi q_n) \pmod 1, \\ q_{n+1} &= q_n + p_{n+1} \pmod 1, \end{aligned} \tag{1}$$

where k is a parameter that measures the strength of the perturbation. This stroboscopic map is generated by the time-dependent Hamiltonian

$$H(q,p,t) = p^2/2 + k/(2\pi)^2 \cos(2\pi q) \sum \delta(t-n). \tag{2}$$

Phase space portraits for $k = 0.01, 0.25, 0.55$, and 1.21 are shown in Fig. 1. For very small k [Fig. 1(a)], the dynamics is approximately integrable, where p is nearly constant and we can see the emergence of the 1:1 resonance in the vicinity of $(q,p) = (1/2,0)$ and $(1/2,1)$. We note that for $k = 0$ and for $p = a/b$ a rational number (a and b integers), the evolution is periodic, that is, the orbits are periodic and nonisolated. These POs are the origin of the nonlinear resonances when $k \neq 0$.

For greater k, we can see the formation of other nonlinear resonances such as 2:1 (the one of period 2) near $p = 1/2$ and 3:1 near $p = 1/3$ and $p = 2/3$ [Figs. 1(b) and 1(c)]. The increase of k results in the formation of chaotic areas that can eventually cover all of the phase space. This is shown in Fig. 1(d). Although the chaotic sea covers a great portion of the phase space for $k = 1.21$, nonlinear 1:1, 2:1, and 3:1 resonances survive this amount of perturbation.

The quantized version of Eq. (1) is provided by the unitary time-evolution operator [18]

$$\psi_{n+1} = \hat{U}\psi_n = \exp\left[-i\frac{\hat{p}^2}{2\hbar}\right]\exp\left[-i\frac{k\cos(2\pi\hat{q})}{\hbar}\right]\psi_n. \tag{3}$$

The periodic nature of the phase space implies that wave functions should be periodic in both position and momentum representations. Then the Hilbert space has a finite dimension N that is related to the Planck constant as $h = 1/N$. As N takes increasing values, the semiclassical limit is reached.

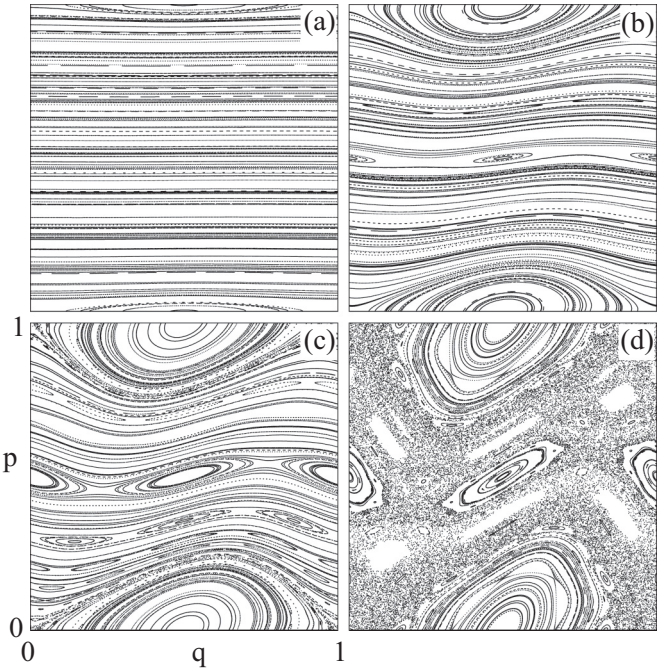

FIG. 1. Classical phase space for the standard map (1) for (a) $k = 0.01$, (b) $k = 0.25$, (c) $k = 0.55$, and (d) $k = 1.21$.

The evolution operator of Eq. (3) in a position representation reads [23]

$$\begin{aligned} U_k(n',n,\alpha_q,\alpha_p) = \frac{1}{N}\exp\left[-\mathrm{i}N\frac{k}{2\pi}\cos\left(\frac{2\pi}{N}(n+\alpha_q)\right)\right] \\ \times \sum_{j=0}^{N-1}\exp\left[-\frac{\mathrm{i}\pi}{N}(j+\alpha_p)^2\right] \\ \times \exp\left[\frac{2\pi\mathrm{i}}{N}(j+\alpha_p)(n-n')\right], \end{aligned} \tag{4}$$

where α_q and α_p are fixed, arbitrary real numbers between 0 and 1 ($2\pi\alpha_q$ and $2\pi\alpha_p$ are called Floquet angles). In this paper we use $\alpha_q = \alpha_p = 0$.

III. NONLINEAR RESONANCE IN THE QUANTUM SPECTRA: EIGENPHASES

Our goal is to reveal the quantum manifestation of the classical transition from integrable to mixed dynamics in the standard map that is shown in Fig. 1. In this section we uncover the influence of such a transition in the spectra of eigenvalues of the evolution operator of Eq. (4). This operator is numerically diagonalized for a given N, the number of states of the Hilbert space. Because the evolution operator is a unitary operator, the eigenvalues $\exp(-i\phi)$ are complex numbers with unit norm. We have studied the cases of $N = 20, 40, 80, 160$, and 320. As an example, in Fig. 2 we show the eigenphases ϕ as a function of the perturbation strength k for $N = 80$.

We focus on the 2:1 resonance. It has two islands near $p = 1/2$ (see Fig. 1). The first step is to find the family of states that exists in the vicinity of the resonance [16,17]. This is straightforward for $k \approx 0$, where the evolution operator is

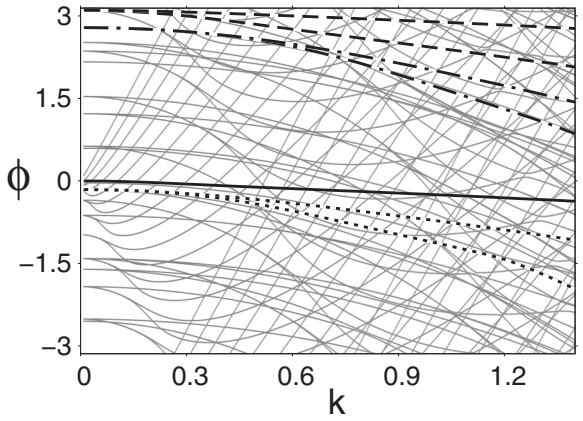

FIG. 2. Correlation diagram for the eigenphases of the quantized standard map with $N = 80$ as a function of the perturbation parameter k. States that for $k = 0$ have $p = 1/2 \pm l/80$ with $l = 0$, 1, 2, and 3 are highlighted. The state with $l = 0$ is plotted with a thick solid black line, the pair of states with $l = 1$ are plotted with dashed lines, the states with $l = 2$ are plotted with dotted lines, and the states with $l = 3$ are plotted with dash-dotted lines.

approximately

$$U = \exp(-i\hat{p}^2/2\hbar), \tag{5}$$

so its eigenstates are the momentum eigenstates $\hat{p}|i\rangle = i/N|i\rangle$ with $i = 0,1,\ldots,N-1$. For N even, the state with eigenvalue $p = 1/2$ is the nearest to the resonance. Then we have a pair of states with eigenvalues $p = 1/2 \pm l/N$ with $l = 1,2,\ldots$, which have degenerate eigenphases and depart from the resonance as l grows. For $k > 0$ the degeneracy breaks down, the eigenphases separate from each other, and the pair of states that are localized in momentum are coupled.

We want to know the behavior of these pairs of states when the parameter $k \neq 0$. For this reason we use the method developed in Ref. [17] to follow eigenstates with definite localization properties. Let us consider an eigenstate of the evolution operator $|\phi_i(k)\rangle$ that for very small perturbation $k = k_0$ has a specific localization. Then we associate a perturbed one with $k = k_0 + \delta k$, if the overlap $\langle\phi_i(k_0)|\phi_j(k_0+\delta k)\rangle$ is the maximum of all $j = 0,1,\ldots,N-1$. This procedure is repeated for perturbations $k = k_0 + n\delta k$ with $n = 2,\ldots,n_{\max}$ an integer. Thus, we have associated a series of perturbed states and eigenphases with the unperturbed one. We note that the value of δk is very important for the success of the method. If δk is very small, an avoided crossing with another state changes the localization of the state that we are following. On the contrary, if δk is very large, the method also fails because the localization properties of the state get lost [17].

First, we consider the case of $N = 80$. In Fig. 2 the eigenphases of the evolution operator of Eq. (1) as a function of the perturbation parameter k are plotted. The states that at $k = 0$ have $p = 1/2 \pm l/N$ for $l = 0$, 1, 2, and 3 are highlighted. The evolution of the eigenphases as a function of k was obtained using the described method. We can see that except for the state with $p = 1/2$ at $k = 0$, all other pairs of states are degenerate at $k = 0$ and separate as the perturbation increases. We are going to show that such splittings can be described using a semiclassical theory.

The semiclassical study of eigenphase gaps between states localized in unperturbed tori due to nonlinear resonances was considered in Refs. [9,10,24]. The first step is to obtain, using secular perturbation theory, the time-independent Hamiltonian that describes the classical motion in the vicinity of a resonance [24,25]

$$H_{r:s}(I,\theta) = H_0(I) - \Omega_{r:s} I + \sum_{l=1}^{\infty} 2V_{r,l}(I_{r:s})\cos(lr\theta + \phi_l), \tag{6}$$

where $H_0(I)$ an integrable approximation of the Hamiltonian of the map, $I_{r:s}$ is the action of the resonance, and $\Omega_{r:s} = \frac{dH_0}{dI}|_{I_{r:s}}$ [10]. The effective Hamiltonian [Eq. (6)] can be reduced to a pendulumlike form

$$H_{r:s}(I,\theta) \simeq \frac{(I - I_{r:s})^2}{2m_{r:s}} + 2V_{r:s}\cos(r\theta + \phi_1), \tag{7}$$

where the effective mass parameter $m_{r:s} = [d^2H_0/dI^2(I_{r:s})]^{-1}$ and only the first term for $l = 1$ [$V_{r:s} \equiv V_{r,1}(I_{r:s})$] was included [10–12]. This last assumption is supported by the fact that $V_{r,l}$ decays exponentially with l and the multistep process generated by the first harmonic $V_{r,1}$ has, in the semiclassical limit $\hbar \to 0$, a stronger amplitude than a single-step process generated by the corresponding higher harmonic $V_{r,l}$ (see Refs. [10,12] for details).

The parameters $m_{r:s}$, $I_{r:s}$, and $V_{r:s}$ that characterize $H_{r:s}$ [Eq. (7)] can be obtained from the classical dynamics without explicitly using the functional form of the integrable H_0 that approximately reproduces the regular motion in the islands. All these quantities are connected by the equations obtained in Refs. [11,26],

$$I_{r:s} = \frac{1}{4\pi}(S^+_{r:s} + S^-_{r:s}), \tag{8}$$

$$\sqrt{2m_{r:s}V_{r:s}} = \frac{1}{16}(S^+_{r:s} - S^-_{r:s}), \tag{9}$$

$$\sqrt{\frac{2V_{r:s}}{m_{r:s}}} = \frac{1}{r^2}\arccos(\mathrm{tr}M_{r:s}/2), \tag{10}$$

where $M_{r:s}$ is the monodromy matrix of a stable PO of the resonance and $S^+_{r:s}$ and $S^-_{r:s}$ are phase space areas that are enclosed by the outer and inner separatrices of the resonance, respectively. Shown in the inset of Fig. 3 is a picture of the relevant phase space areas of the 2:1 resonance.

Let us now compute the splitting of the eigenphases between two degenerate states that are symmetrically located around an $r:s$ resonance. The effective Hamiltonian [Eq. (7)] couples unperturbed states with quantum numbers that differ by r. Then two degenerate states with quantum number difference rl, with l an integer, interact via the effective Hamiltonian [Eq. (6)] that in the unperturbed base is a tridiagonal matrix with diagonal elements

$$E_i = \hbar^2[(i - l/2)r]^2/2m_{r:s}, \tag{11}$$

with $i = 0,1,\ldots,l$, and the nondiagonal elements are $V_{r:s}$. Applying standard perturbation theory in the limit $V_{r:s} \to 0$, we obtain for the level splitting between the states with energy

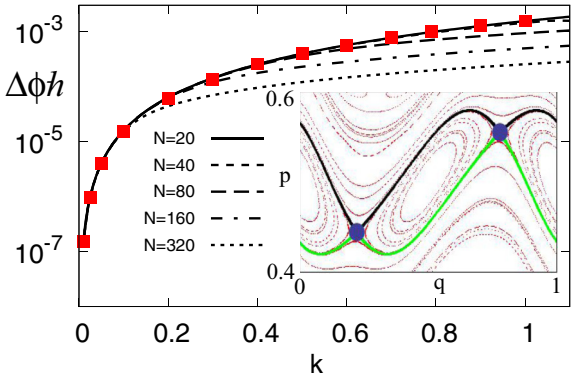

FIG. 3. (Color online) Eigenphase difference (scaled with $\hbar$) as a function of the perturbation strength k for states that at $k = 0$ have $p = 1/2 + 1/N$ and $p = 1/2 - 1/N$ with $N = 20$ (solid line), 40 (short-dashed line), 80 (long-dashed line), 160 (dash-dotted line), and 320 (dotted line). The semiclassical approximation given by Eq. (15) is plotted with red closed squares. Inset: Region of the classical phase space for $k = 0.7$ that has been used to compute the semiclassical approximation. The unstable periodic orbit associated with the 2:1 resonance is plotted with blue circles. The phase space area $S^+_{2:1} - S^-_{2:1}$ is the region enclosed by the black and green lines.

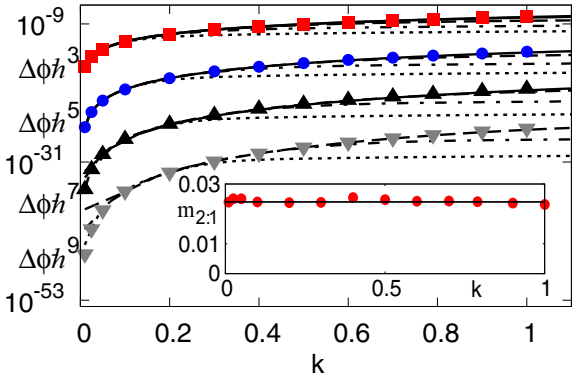

FIG. 4. (Color online) Eigenphase difference (scaled with $\hbar^{2l-1}$) as a function of the perturbation strength for the states that at $k = 0$ have $p = 1/2 \pm l/N$ ($l = 2, 3, 4$, and 5). The dimension of the Hilbert space is $N = 20$ (solid line), 40 (short-dashed line), 80 (long-dashed line), 160 (dash-dotted line), and 320 (dotted line). The semiclassical approximation (15) is plotted with closed symbols [($l = 2$ (squares), 3 (circles), 4 (upward triangles), and 5 (downward triangles)]. Inset: $m_{2:1}$ as a function of k. The solid black line plots $m_{2:1} = 0.024$.

E_0 and E_l,

$$\Delta E = 2V_{r:s} \prod_{i=1}^{l-1} [V_{r:s}/(E_0 - E_i)]. \tag{12}$$

The eigenphase splitting $\Delta\phi$ is obtained using $\Delta\phi = \Delta E/\hbar$ and Eqs. (11) and (12). We finally obtain

$$\Delta\phi = \frac{2V^l_{r:s}(2m_{r:s})^{l-1}}{[(l-1)!]^2\hbar^{2l-1}r^{2l-2}}. \tag{13}$$

The parameters $m_{r:s}$ and $V_{r:s}$ are obtained from the monodromy matrix $M_{r:s}$ and the phase space area $S^+_{r:s} - S^-_{r:s}$. Note that in the regime of large $l \gg 1$, in which we approximate $(l-1)!^2 \simeq (l/e)^{2l}2\pi/l$, Eq. (13) is identical to the semiclassical Wentzel-Kramers-Brillouin (WKB) expression

$$\Delta\phi^{(\mathrm{WKB})} = \frac{\omega}{\pi}e^{-\sigma/\hbar} \simeq \frac{lr^2\hbar}{2\pi m_{r:s}}\left(\frac{2e^2 m_{r:s}V_{r:s}}{l^2r^2\hbar^2}\right)^l \tag{14}$$

for the eigenphase splitting between the states with the momenta $p = 1/2(1 \pm \Delta p)$ with $\Delta p = lr/N$, where we have $\omega = r\Delta p/4\pi m_{r:s} = r\hbar/2m_{r:s}$ for the effective frequency of tunneling attempts and $\sigma = -\Delta p/2\pi r \ln[8\pi^2e^2m_{r:s}V_{r:s}/(\Delta p)^2] = -l\hbar\ln[2e^2m_{r:s}V_{r:s}/(lr\hbar)^2]$ for the imaginary action associated with the complex tunneling path [10].[1]

We test Eq. (13) to compute the splittings produced by the 2:1 resonance between the states that are degenerate at $k = 0$ and have $p = 1/2 \pm l/N$ (l an integer). For this resonance we can go one step further and compute the scaling of $V_{r:s}$ with k. What helps us here is the fact that we know precisely the positions of the periodic points associated with the 2:1 resonance. These periodic points become fixed points under a twofold iteration of the standard map. Taking the stable periodic point at $k = 0$, $(p,q) = (1/2,0)$ and linearizing the dynamics of the twice iterated standard map in the vicinity of this point yields the monodromy matrix

$$M_{2:1} = \begin{pmatrix} 1-k & -k^2 \\ 2-k & 1+k-k^2 \end{pmatrix}.$$

As expected $\det(M_{2:1}) = 1$ and we find that $\mathrm{Tr}(M_{2:1}) = 2 - k^2$. Then, using Eq. (10) we obtain that $V_{2:1} = m_{2:1}k^2/32$. Finally, using this expression and Eq. (13), the eigenphase splitting $\Delta\phi$ for the resonance 2:1 results

$$\Delta\phi = \frac{k^{2l}m^{2l-1}_{r:s}}{[(l-1)!]^2\hbar^{2l-1}2^{6l-2}}. \tag{15}$$

We have obtained $m_{r:s} \approx 0.024 \approx 1/(2\pi)^2$ (see the inset of Fig. 4) using Eqs. (9) and (10) and computing numerically the phase space areas $S^+_{r:s}$ and $S^-_{r:s}$.

The splittings $\Delta\phi$ for $l = 1$ are shown in Fig. 3. The quantum splittings were computed for $N = 20$, 40, 80, 160, and 320. The semiclassical result is plotted with symbols. We see very good agreement between the quantum calculations and the semiclassical prediction. We note that Eq. (13) works also to describe the splittings for $l = 1$, 2, and 3 in the Harper map (not shown). In the limit $N \to \infty$ and for fixed l, the semiclassical expression works when $k \to 0$. In this limit, we are moving closer and closer to the 2:1 resonance's center and then higher-order resonances, which can generally modify tunneling rates in a drastic manner [10–14,27], practically do not enter into consideration.

In Fig. 4 we plot the splittings for $l = 2$, 3, 4, and 5. The semiclassical prediction also works very well for all these cases for small perturbation strength k. We can see that for large N

[1]Note that the latter imaginary action is *a priori* a purely classical quantity that results from the properties of the complexified invariant phase-space curves with the momenta $p = 1/2(1 \pm \Delta p)$. However, choosing $\Delta p = lr/N$, as we effectively do in our calculations, will introduce an effective $\hbar$ dependence in this imaginary action, which in turn changes the scaling of the WKB splitting [Eq. (14)] with $\hbar$.

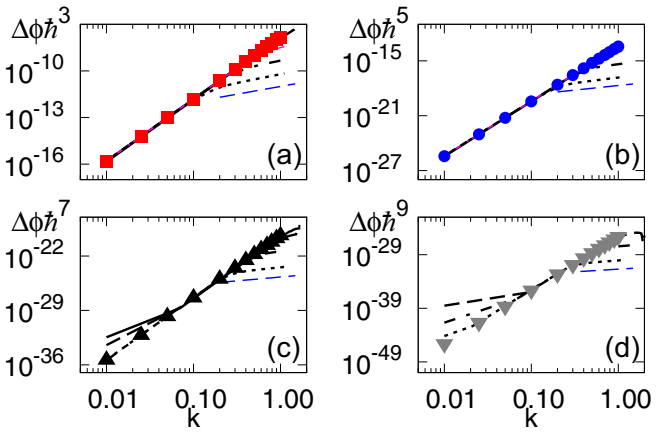

FIG. 5. (Color online) Eigenphase difference (scaled with $\hbar^{2l-1}$) as a function of the perturbation strength for the states that at $k = 0$ have $p = 1/2 \pm l/N$ on a log-log scale and (a) $l = 2$, (b) $l = 3$, (c) $l = 4$, and (d) $l = 5$. The dimension of the Hilbert space is $N = 20$ (solid line), 40 (short-dashed line), 80 (long-dashed line), 160 (dash-dotted line), and 320 (dotted line). The semiclassical approximation (15) is plotted with closed symbols. A linear function is plotted with a blue dashed line. Deviations from the semiclassical power-law behavior at low values of k occur due to the fact that in that regime couplings via the central pendulum feature at $q = 1/2$ and $p = 0$ become more dominant than resonance-assisted couplings via the 2:1 resonance. At high values of k, the states become localized within the islands of the 2:1 resonance. The splitting is then expected to increase linearly with the perturbation strength.

the rescaled splittings saturate at some given value of k and do not increase further with k. In Fig. 5 we plot on a log-log scale the splittings for $l = 2$, 3, 4, and 5 as a function of k to show in more detail the departure from the semiclassical growth law given by Eq. (15). We can clearly see two regimes, a power law of Eq. (15) for small k and a linear regime that is shown with a dashed line as a guide for the eye. The occurrence of this linear regime can be straightforwardly explained by the fact that the two states that are involved in the tunneling process move inside the 2:1 resonance islands in the limit of large N and become Einstein-Brillouin-Keller localized within the islands. Their associated eigenphase splitting will then be given by the local oscillation frequency $\omega_{2:1}$ around the center of the 2:1 island and the latter is evaluated as $\omega_{2:1} = 2(2V_{2:1}/m_{2:1})^{1/2} = k/2$ for the standard map. In the next section a connection of this linear regime with the morphology of the wave functions of these states will be given. We note that the deviation for very low k that is visible in Fig. 5 is due to the fact that in this regime the 1:1 resonance at $p = 0$ and $q = 1/2$ provides a more dominant coupling mechanism than the 2:1 resonance, especially if the involved states are located relatively far away from the 2:1 resonance (i.e., for large l).

IV. MORPHOLOGY OF EIGENFUNCTIONS

In the previous section we focused on the spectral manifestation of the nonlinear 2:1 resonance. We showed that pairs of states with $p = 1/2 + l/N$ and $p = 1/2 - l/N$ (l an integer) at $k = 0$ are degenerate, while for $k > 0$ the states depart from each other as k grows due to the resonance 2:1. In this section we study the morphology of these states as the perturbation departs from $k = 0$.

The morphology of the eigenfunctions is studied using the Husimi distribution, a quasiprobability distribution in phase space. An interesting feature of such a representation for quantum maps is that it has exactly N zeros in the unit square [28]. In Fig. 6 the Husimi distributions of the highlighted states of Fig. 2 for $k = 0.01$, 0.25, 0.57, and 1.21 are shown. The left column [labeled with (1)] shows the eigenstates for $k = 0.01$. The state (1a) corresponds to the state that at $k = 0$ has $p = 1/2$. It is clearly localized in the vicinity of this value of p as expected. What is unexpected is the behavior of the other states. We can clearly see that states (1b), (1c), (1d), (1e), (1f), and (1g) are also localized near $p = 1/2$ but a series of zeros is clearly visible in the region where the values of the Husimi distribution are large. Inspecting those states more carefully, we note that states (1b), (1d), and (1f) have zeros on the unstable PO corresponding to the 2:1 resonance and have 0, 2, and 4 zeros, respectively, in the region of the islands of the resonance. On the contrary, states (1c), (1e), and (1g) have a maximum on the unstable PO and 2, 4, and 6 zeros in the region of the islands. This behavior of the zeros is also observed for greater values of k and does not depend on the value of N. This surprising behavior of zeros was also shown in the Harper map [16,17]; however, it is important to note a different aspect of that system. In the case of the Harper map for small values of the perturbation, each unperturbed state has a different eigenphase slope [16,17]. Then unperturbed states that exist around invariant tori are mixed when they interact in an avoided crossing if their quantum numbers differ by a multiple of the order of the classical resonance. So, the localized states that are observed in the standard map for all values of $k > 0$ is developed in the Harper map only in the vicinity of avoided crossings. This fact makes the standard map more suitable for these studies because it is no longer needed to find the precise location of the ACs.

To see the behavior of the localization of the zeros in more detail, we plot in Fig. 7 the natural logarithm of the Husimi distribution $\ln[H(q,p)]$ of the state that is plotted with a blue line in Fig. 2 and corresponds to the second row of Fig. 6 [states (1d), (2d), (3b), and (4d)]. In Fig. 7 we also plot the location of the unstable PO. We can clearly see that for $k = 0.01$ [Fig. 7(a)] the positions of the zeros of the Husimi distribution agree very well with the position of the unstable PO (center of the black circles). We note that the zeros of the Husimi distribution are located in the isolated minima of the function [for example, blue spots in Fig. 7(a) of 6]; however, as soon as k increases [Figs. 7(b)–7(d)] the agreement is no longer valid.

We remark that we have studied other values of N (dimension of the Hilbert space) and the same system was observed. In Fig. 8 we show an example for $N = 320$. It shows the Husimi distribution of the pairs of states that at $k = 0$ have $p = 1/2 \pm 3/320$ for $k = 0.01$, 0.1, 0.25, 0.57, and 1.11. We can see that the states plotted in the left column, labeled (1a)–(1e), have 2 zeros in the unstable PO and 4 zeros in the islands (2 zeros in each island). The other states, plotted in the right column [panels (2a)–(2e)], have 6 zeros in the islands (3 in each one). In Fig. 5(b) (black line) we have plotted the eigenphase splitting of these states. We can see that states (1d), (1e), (2d), and (2e) correspond to the

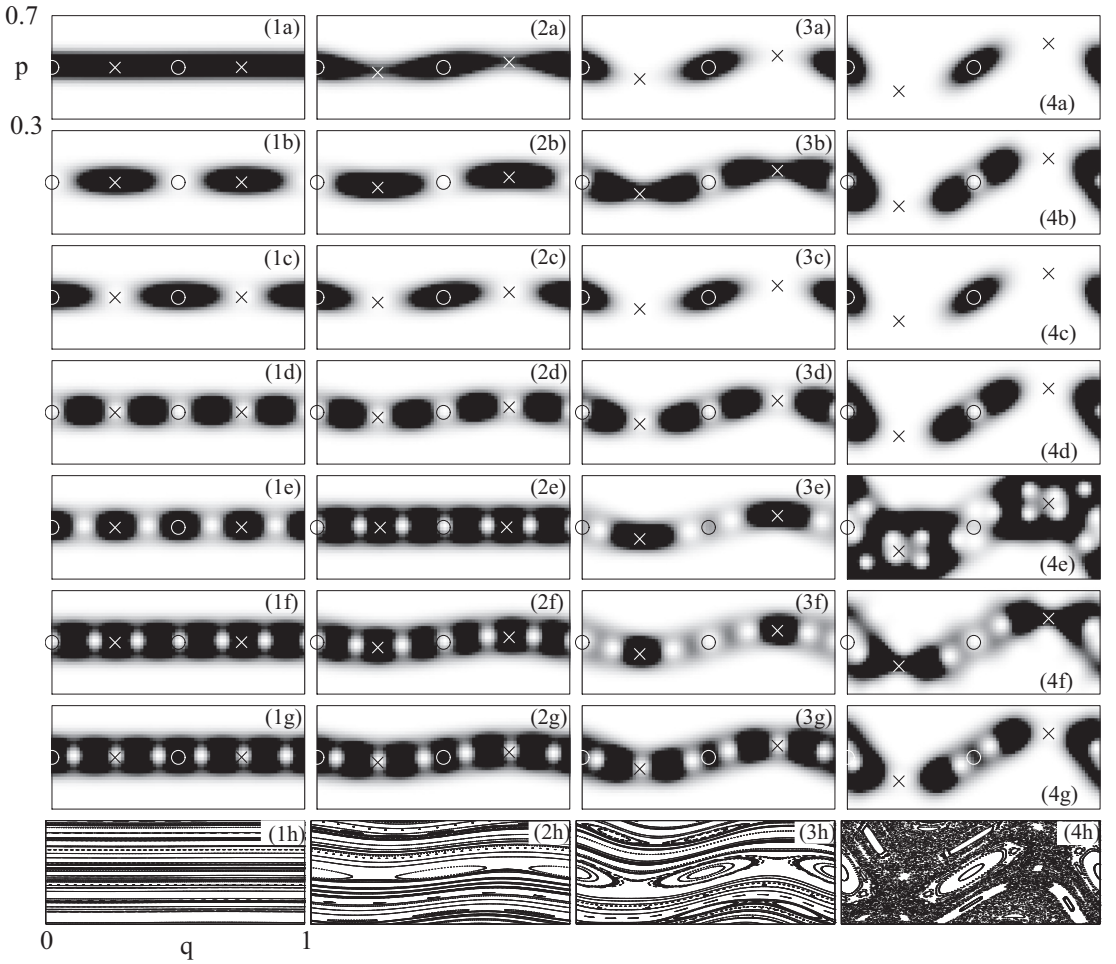

FIG. 6. Husimi distribution $H(q,p)$ of the highlighted states of Fig. 2 at $k = 0.01$ (labeled 1), 0.25 (labeled 2), 0.57 (labeled 3), and 1.21 (labeled 4). States labeled (a) correspond to states that have $p = 1/2$ at $k = 0$ (thick solid black line in Fig. 2), states (b) and (c) correspond to states that have $p = 41/80$ and $p = 39/80$ at $k = 0$ ($l = 1$, dashed lines in Fig. 2), states (d) and (e) correspond to states that have $p = 42/80$ and $p = 38/80$ at $k = 0$ ($l = 2$, dotted lines in Fig. 2), and states (f) and (g) correspond to states that have $p = 43/80$ and $p = 37/80$ at $k = 0$ ($l = 3$, dash-dotted lines in Fig. 2). The stable and unstable periodic orbits of the resonance 2:1 are plotted with circles and crosses. The corresponding areas of phase space are plotted in (h).

linear regime of $\Delta\phi$. These states are localized within the two islands of the 2:1 resonance. The resulting eigenphase splitting is then the energetic difference between the nth and the $(n+1)$th excited eigenstates within one of the two resonance islands for some $n > 0$ that should be proportional to the local oscillation frequency around the stable fixed point of the 2:1 resonance. Further increasing the size of the islands generally gives rise to a larger number of states being localized within the islands, hence more and more states depart from the growth behavior predicted by Eq. (15). Their splittings are still expected to increase with increasing perturbation, because the local oscillation frequency is generally enhanced with increasing size of the island. This linear growth, however, is much weaker than the power law increase of splittings [Eq. (15)] due to enhanced tunneling between states that are anchored outside the islands.

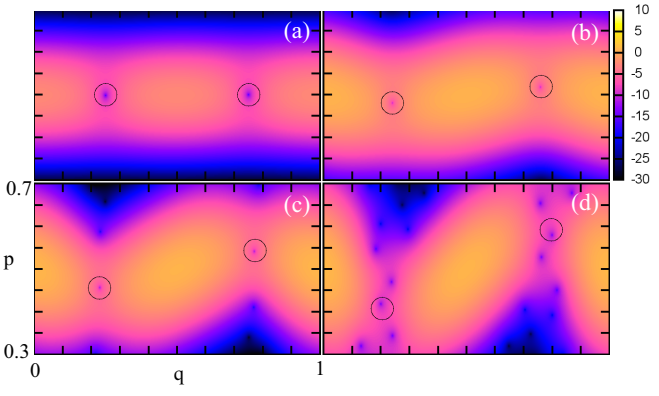

FIG. 7. (Color online) Logarithm of the Husimi distribution $H(q,p)$ of the states (1b), (2b), (3b), and (4b) of Fig. 6. The location of the unstable periodic orbit of the resonance 2:1 is indicated with circles. (a) $k = 0.01$, (b) $k = 0.25$, (c) $k = 0.57$, and (d) $k = 1.21$.

In conclusion, we have shown that the states near a nonlinear r:s resonance have a definite morphology. Pairs of states that are degenerate at $k = 0$ separate as k increases: One of the states has rl zeros inside the islands with $l = 1,2,\ldots$ (l zeros in each island) and the other state has a zero on each point of the unstable periodic orbit of the nonlinear resonance and $r(l-l)$ zeros inside the islands ($l-1$ in each one).

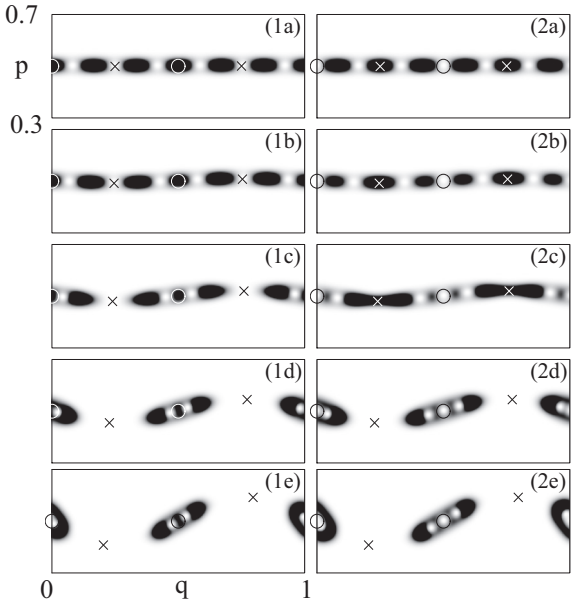

FIG. 8. Husimi distribution $H(q,p)$ of the states that at $k = 0$ have $p = 1/2 \pm 3/320$ for $N = 320$: (1a) and (2a) $k = 0.01$, (1b) and (2b) $k = 0.1$, (1c) and (2c) $k = 0.25$, (1d) and (2d) $k = 0.57$, and (1e) and (2e) $k = 1.11$. The stable and unstable periodic orbits of the resonance 2:1 are plotted with circles and crosses.

V. CONCLUSION

In this paper we have studied the quantum manifestations of the classical transition from integrable to mixed dynamics in a paradigmatic standard map. We have shown a clear systematic behavior that nonlinear resonances imprint to the eigenphases and eigenstates of the evolution operator of the map. The nonlinear resonance mixes degenerate unperturbed states that exist in its vicinity. The perturbation that breaks the degeneracy of unperturbed states can be modeled by a time-independent Hamiltonian whose parameters can be obtained from the classical dynamics. This Hamiltonian that is obtained using secular perturbation theory describes the classical motion in the vicinity of the resonance. Using this integrable Hamiltonian and perturbation theory, we have obtained a semiclassical expression for the gaps between the eigenphases of perturbed states. We have numerically shown in the standard map that this expression works very well to describe the quantum results not only in the limit of $\hbar \to 0$. We also note that the semiclassical expression works very well in the Harper map. These findings can be useful in predicting resonance assisted tunneling rates also in a more generic case of nonresonant transitions across the island chain, which is a topic for further investigation.

The perturbed states have well defined localization properties. One of the states is localized in the island chain and the other on the corresponding unstable PO. The Husimi distribution of the state that is localized in the islands has a zero in each point of the unstable periodic orbit of the nonlinear resonance and $r(l-1)$ zeros inside the islands ($l-1$ in each one, with l an integer). The other state has rl zeros inside the islands. We note that in the Harper map the same morphology of wave functions was shown, but in the center of avoided crossings [16,17] when the unperturbed states are mixed.

The transition from integrable to mixed dynamics is ubiquitous in Hamiltonian systems and its quantum manifestation now attracts a renewed interest in optical microcavities [29]. Such devices were in general seated in the region of mixed classical dynamics and were shown to be important for quantum phenomena such as scarlike modes [30–32]. Although this system has an open dynamics, our results could be of importance in obtaining a desired localization of the output directionality.

ACKNOWLEDGMENTS

D.A.W. thanks Marcos Saraceno for stimulating discussions and acknowledge the support from UBACyT (Grant No. 20020130100406BA) and ANPCyT (Grant No. PICT-2010-02483).

[1] P. Cvitanović, R. Artuso, R. Mainieri, G. Tanner, and G. Vattay, *Chaos: Classical and Quantum* (Niels Bohr Institute, Copenhagen, 2009).
[2] *Chaos and Quantum Physics*, edited by M.-J. Giannoni, A. Voros, and J. Zinn-Justin, Les Houches Summer School of Theoretical Physics, Session LII, 1989 (North-Holland, Amsterdam, 1991).
[3] H. J. Stöckman, *Quantum Chaos: An Introduction* (Cambridge University Press, Cambridge, 1999).
[4] O. Bohigas, M. J. Giannoni, and C. Schmit, Phys. Rev. Lett. **52**, 1 (1984).
[5] S. Müller, S. Heusler, P. Braun, F. Haake, and A. Altland, Phys. Rev. Lett. **93**, 014103 (2004).
[6] R. Jalabert, Scholarpedia (to be published).
[7] V. I. Arnold, S. M. Gusein-Sade, and A. N. Varchenko, *Mathematical Aspects of Classical and Celestial Mechanics* (Springer, Berlin, 2006).
[8] G. D. Birkhoff, Trans. Am. Math. Soc. **14**, 14 (1913).
[9] L. Bonci, A. Farusi, P. Grigolini, and R. Roncaglia, Phys. Rev. E **58**, 5689 (1998).
[10] O. Brodier, P. Schlagheck, and D. Ullmo, Phys. Rev. Lett. **87**, 064101 (2001); Ann. Phys. (N.Y.) **300**, 88 (2002).
[11] C. Eltschka and P. Schlagheck, Phys. Rev. Lett. **94**, 014101 (2005).
[12] P. Schlagheck, A. Mouchet, and D. Ullmo, in *Dynamical Tunneling—Theory and Experiment*, edited by S. Keshavamurthy and P. Schlagheck (CRC, Boca Raton, 2011).
[13] S. Löck, A. Bäcker, R. Ketzmerick, and P. Schlagheck, Phys. Rev. Lett. **104**, 114101 (2010).
[14] S. Gehler, S. Löck, S. Shinohara, A. Bäcker, R. Ketzmerick, U. Kuhl, and H.-J. Stöckmann, Phys. Rev. Lett. **115**, 104101 (2015).
[15] P. M. Koch and K. A. H. van Leeuwen, Phys. Rep. **255**, 289 (1995).

[16] D. A. Wisniacki, M. Saraceno, F. J. Arranz, R. M. Benito, and F. Borondo, Phys. Rev. E **84**, 026206 (2011).
[17] D. A. Wisniacki, Europhys. Lett. **106**, 60006 (2014).
[18] B. Chirikov and D. Shepelyansky, Scholarpedia **3**, 3550 (2008).
[19] B. Chirikov, Phys. Rep. **52**, 263 (1979).
[20] F. M. Izraelev, Physica D **1**, 243 (1980).
[21] G. Casati, B. V. Chirikov, and D. L. Shepelyansky, Phys. Rev. Lett. **53**, 2525 (1984).
[22] D. L. Shepelyansky and A. D. Stone, Phys. Rev. Lett. **74**, 2098 (1995).
[23] A. Lakshminarayan, Phys. Rev. E **64**, 036207 (2001).
[24] A. M. Ozorio de Almeida, J. Phys. Chem. **88**, 6139 (1984).
[25] A. J. Lichtenberg and M. A. Lieberman, *Regular and Stochastic Motion* (Springer, New York, 1983).
[26] S. Tomsovic, M. Grinberg, and D. Ullmo, Phys. Rev. Lett. **75**, 4346 (1995).
[27] Y. Hanada, A. Shudo, and K. S. Ikeda, Phys. Rev. E **91**, 042913 (2015).
[28] P. Leboeuf and A. Voros, J. Phys. A **23**, 1765 (1990).
[29] H. Cao and J. Wiersig, Rev. Mod. Phys. **87**, 61 (2015).
[30] J. Wiersig, Phys. Rev. Lett. **97**, 253901 (2006).
[31] H. Kwak, Y. Shin, S. Moon, S.-B. Lee, J. Yang, and K. An, Sci. Rep. **5**, 9010 (2015).
[32] C.-H. Yi, H.-H. Yu, J.-W. Lee, and C.-M. Kim, Phys. Rev. E **91**, 042903 (2015).